Effect of salt spray ageing on the fracture of composite-to-metal bonded joints

M.M. Arouche, M.N. Saleh, S. Teixeira de Freitas, Silvio DE BARROS

International Journal of Adhesion & Adhesives 108 (2021) 102885

Contents lists available at ScienceDirect

International Journal of Adhesion and Adhesives

journal homepage: http://www.elsevier.com/locate/ijadhadh

Effect of salt spray ageing on the fracture of composite-to-metal bonded joints

M.M. Arouche [a,b], M.N. Saleh [b], S. Teixeira de Freitas [b,*], S. de Barros [a,c]

[a] Federal Center for Technological Education of Rio de Janeiro – CEFET/RJ, Av. Maracanã 229, 20271-110, Rio de Janeiro, Brazil
[b] Delft University of Technology, Kluyverweg 1, 2629HS, Delft, Netherlands
[c] GeM Institute, UMR 6183 CNRS, CESI, Saint-Nazaire, France

ARTICLE INFO

Keywords:
Fracture toughness
Bi-material bonded joints
Adhesion
Fractography
Ageing

ABSTRACT

This work investigates the effect of long-term environmental exposure on the performance of composite-to-metal bonded joints. Specimens are manufactured using a carbon-fiber reinforced polymer (CFRP) co-bonded to a steel member with epoxy adhesive and aged in a salt spray chamber. The mixed-mode fracture behavior of the non-aged and aged specimens is assessed using the mixed-mode bending (MMB) test apparatus. The fracture energy is calculated using the finite elements method and an analytical approach, the strain-based method (SBM). The SBM showed to be a simple and accurate method to obtain the total fracture energy and the fracture mode ratio of the bi-material specimen. Ageing increased the fracture toughness at crack initiation by 27% for specimens loaded at 20% mode II and 7% for specimens loaded at 15% mode II. This can be related to the shear behavior and plasticization of the adhesive material. During crack propagation, the fracture toughness remained similar for specimens loaded at 20% mode II and decreased by 15% in specimens loaded at 15% mode II. Fractography analysis together with chemical characterization showed that the penetration of moisture at the edges of the fracture surface produced adhesive failure in these regions affected by moisture. Moreover, the failure mode at the unaffected regions of the fracture surface shifted from cohesive to a combination of thin-layer cohesive and adhesive failure after ageing. The results contributed to describe the effect of ageing on the fracture behavior of bonded materials.

1. Introduction

The requirement of lightweight structures has encouraged the introduction of composite materials in industrial applications. Advanced composite materials, which usually consist of a polymer matrix reinforced with continuous fibers, can provide high strength with a relatively low weight and thus enable superior structural performance to be achieved. Novel design of structures can be developed as manufacturers replace traditional materials with advanced composite materials. Budhe et al. [1] expresses that adhesive bonding technology is generally the preferred joining method for composite parts as it provides enhanced stress transfer mechanisms and design flexibility. In addition, the design optimization of these structures requires the understanding of several parameters, such as substrates to be bonded, service conditions and area of application. The work of Oudad et al. [2] showed that moisture absorption caused reduction of structural performance of bonded composite repairs in aircraft structures. Lau and Büyüköztürk [3] verified that moisture conditioning resulted in a significant decrease in the performance of concrete/epoxy bond. Viana et al. [4] included that wet environment is also one of the main factors that affect the strength of adhesive joints in vehicles. These environmental parameters affect the long-term performance of bonded structures and thus represent a critical barrier to the expansion of their applications.

Several authors studied the effect of environmental degradation on the tensile strength of adhesive bonded joints. Early investigation in metal single lap joints (SLJs) performed by Brewis et al. [5] showed that the moisture penetrates in the joint by diffusion through the adhesive, and consequently the degradation relates with time and tends to level off at the saturation level. Pethrick [6] described the main contributions to the loss of strength of metal bonded joints to be the hydrodynamic displacement at the interface, adhesive plasticization and corrosion at the substrates. Sugiman et al. [7] showed that residual stresses due to thermal and swelling strains in the adhesive layer have no significant effect on the joint strength. Papanicolaou et al. [8] verified that the

* Corresponding author.
E-mail address: s.teixeiradefreitas@tudelft.nl (S. Teixeira de Freitas).

https://doi.org/10.1016/j.ijadhadh.2021.102885

Available online 26 April 2021

Table 1
Mechanical properties of the materials.

Material	Elastic Modulus		Poisson Ratio	Yield/ Tensile Strength	Elongation at Break
	E, E_1 (GPa)	E_2 (GPa)	ν, ν_{12}	σ (MPa)	ε (%)
Steel	200	–	0.27	250	–
Composite 0/90	82	10	0.24	620	3.6
Adhesive	2.25	–	0.38	50	0.8

strength of metal SLJs decreases as a consequence of salt spray ageing.

Regarding composite bonded joints, the work of Park et al. [9] addressed the effect of manufacturing process on the strength of composite SLJs under environmental conditions. They obtained a higher performance of co-cured composite joints in elevated temperatures and wet conditions. Jeong et al. [10] evaluated the effect of secondary bonded joints immersed in tap water and salt water. Results showed an increase of strength in pre-saturated specimens and decrease in specimens with saturated moisture content. The major failure modes of the composite bonded joints were found to be delamination and intralaminar failure of the composite adherend. Moreover, Arouche et al. [11] verified a decrease in the interlaminar adhesion of carbon-epoxy laminates subjected to salt water ageing.

Recently, several works have been carried out on the degradation of bi-material bonded joints between composite and metal adherends. Mariam et al. [12] attested that the tensile strength of dissimilar joints showed to be higher than composite joints due to the different behavior between the permeable composite adherend and impermeable metal adherend under moisture degradation. Arouche et al. [13] and Teixeira de Freitas et al. [14] verified a relation between the reduction of peel strength in composite-to-metal bonded joints and the moisture penetration in salt water and salt spray, as a consequence of the change in the failure mechanism from cohesive to adhesive failure after ageing. Heshmati et al. [15] revealed a higher influence of moisture content on the degradation of a glass-fiber reinforced polymer (GFRP) compared to a carbon-fiber reinforced polymer (CFRP) in composite-to-metal double lap shear (DLS) joints due to the low permeability of the CFRP in comparison with GFRP. The work also showed that the diffusion rate of distilled water is higher than salt water, causing more degradation to the interlaminar strength in short-term immersion. However, with longer exposure times, salt water resulted in more damaging effects to the resin/fiber interface. A study performed by Sugiman et al. [16] obtained a similar outcome regarding the diffusion rate in an epoxy adhesive. Additionally, the diffusion rate showed to be much higher in the fiber direction than the through-thickness direction of unidirectional composites. The effect of salt water under fluctuating condition was more severe than the effect of both distilled and salt water under steady condition. Yang et al. [17] detected the degradation of a laminate due to galvanic coupling developed from corrosion product depositions over steel and exposed carbon fibers. Although these studies provide valuable and insightful information, there remain a number of aspects that require investigation of the mechanical properties of bi-material bonded joints.

Limited work is available on the fracture behavior of bonded materials subjected to environmental conditions. Loh et al. [18] revealed that the fracture energy was primarily associated with the moisture content and independent of test method and time. The experiments of Wylde and Spelt [19] showed that the combined effects of temperature and water caused an initial increase in strength due to plasticization followed by a reduction due to degradation. Ameli et al. [20] tested open-faced epoxy-aluminum specimens and revealed that the fracture toughness decreases as the crack grows closer to the interface for a given level of degradation regardless of the fracture mode ratio. Fernandes et al. [21] evaluated the effect of ageing in metal bonded joints using a secondary bonding method with aged adhesive plates. They detected an increase of the fracture toughness after exposure to salt water due to plasticization of the adhesive, while degradation of the fracture toughness was observed in distilled water as consequence of a substantial reduction of the glass transition temperature. Although the ageing methods previously mentioned are time-efficient, their results may differ from the actual degradation mechanisms in real bonded structures.

Costa et al. [22] observed the degradation of the pure mode I fracture toughness of aluminum bonded joints exposed to moist conditions. In general, aged specimens fail adhesively while non-aged specimens usually show cohesive failure. In the case of composite bonded materials, Markatos et al. [23] detected a considerable reduction of the fracture toughness at crack initiation in bonded CFRP laminates after immersion in de-mineralized water. Interfacial failure also showed to become the dominant failure mode. Fernandes et al. [24] verified a relationship between physical alterations of the adhesive material and

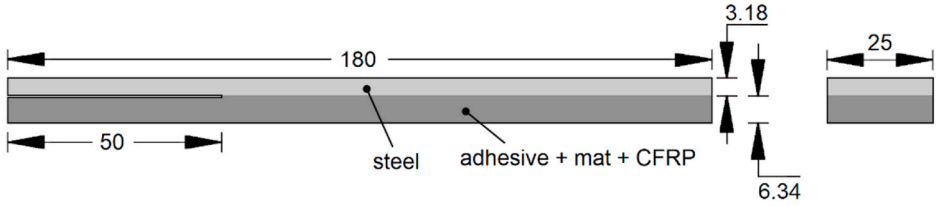

Fig. 1. Specimen geometry (dimensions in millimeters).

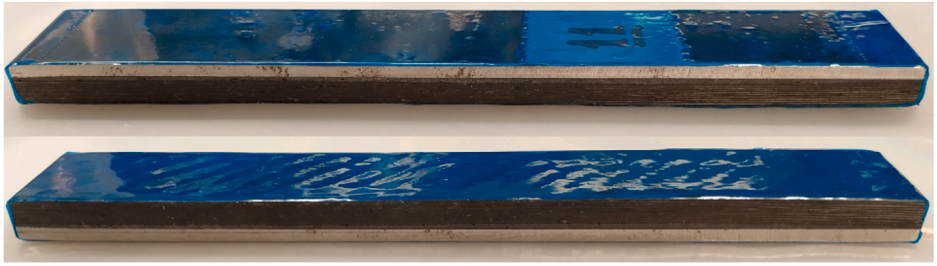

Fig. 2. A specimen prepared for ageing.

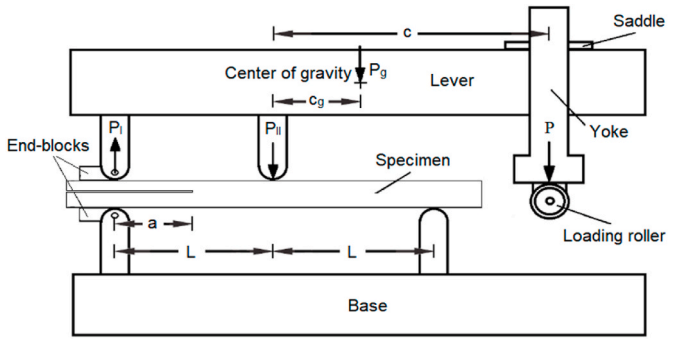

Fig. 3. MMB test scheme.

the reduction of pure mode I and pure mode II fracture energy of composite bonded joints under the effect of moisture. However, these studies address only the pure modes. In real-life applications, cracks in bonded joints propagate in a combination of opening (mode I) and shear (mode II) loadings.

Recently, few authors addressed the effect of moisture on the fracture of symmetric composites. LeBlanc and LaPlante [25] investigated the delamination growth of a carbon-epoxy composite aged in distilled water. The fracture energy increased in pure mode I while the pure mode II and mixed-mode conditions were weakened. Silva et al. [26] obtained similar results for the pure modes using composite bonded joints aged in humid atmosphere. However, specimens tested in mixed-mode conditions presented a reduction in the mechanical properties. Additionally, fracture energy decreased after ageing in salt fog. In general, fracture properties degrade with the exposure time with non-negligible effects at early stages followed by a stabilization trend. However, these studies focused on the quantitative analysis of the fracture toughness. The analysis of failure mechanisms and their association to the degradation of mechanical properties may reveal additional data to improve the design of adhesively bonded structures.

Finally, a review on available literature performed by André et al. [27] revealed insufficient information regarding the fracture of bi-material bonded joints. In this matter, Shahverdi et al. [28] and Arouche et al. [29] successfully applied the mixed-mode bending (MMB) test method for the analysis of dissimilar composite bonded joints and composite-to-metal bonded joints, respectively. The MMB test proved to be a simple and reliable technique to evaluate the fracture performance of dissimilar bonded specimens under mixed-mode loadings. The experimental procedure shows potential to be further extended for the evaluation of the effect of environmental conditions in bi-material bonded joints.

In this work, the effect of long-term environmental exposure on the performance of composite-to-metal bonded joints is investigated. Specimens are manufactured using a CFRP co-bonded to steel with an epoxy adhesive. Samples are aged in a salt spray chamber. The mixed-mode fracture behavior of non-aged and aged specimens is assessed using the MMB test apparatus. The fracture energy is calculated using numerical and analytical approaches. A fracture surface analysis together with a chemical characterization are performed in order to evaluate the failure mechanisms in association with the performance of the bonded joint subjected to environmental exposure.

2. Materials and experiments

2.1. Specimen manufacturing

Composite-to-metal bonded specimens were manufactured in order to simulate the application of a composite repair to a metal structure in offshore industry [29]. A steel plate (ASTM A36) of 3.18 mm thickness was selected for the metal adherend. The steel surface was blasted with steel grit (G-40) and degreased with acetone. An epoxy adhesive (NVT201E, Novatec, Rio de Janeiro, Brazil) with a glass transition temperature (T_g) of 80 °C was applied. One layer of glass fiber chopped strand mat with a density of 300 g/m^2 was inserted between the adhesive and the composite. Bidirectional carbon fiber fabrics (LTC450-C10-C, DEVOLD AMT, Langevåg, Norway) with density of 430 g/m^2 and epoxy lamination resin (PIPEFIX, Polinova S.A., Rio de Janeiro, Brazil) with a T_g of 116 °C and working life of 30 min were selected for the composite adherend. A composite-to-metal plate was manufactured by hand lay up on the treated metal surface. The composite adherend has 10 layers of 0/90° carbon fibers. The first unidirectional carbon ply in contact with the glass fiber mat was placed at the length direction (0°). The adhesive and resin curing process occurred simultaneously in approximately 2 h at room temperature. The properties of the materials were obtained from a previous work [14] and are shown in Table 1.

Specimens were cut from the plates using a bandsaw with a high-speed steel blade and cutting oil. Measurements of width and thickness were obtained with a digital caliper at 30 mm from both ends and at center of the specimens. Specimen geometry is shown in Fig. 1. The specimens have an average width of 25.28 ± 0.18 mm and an average thickness of 9.52 ± 0.19 mm. The average length of 180 ± 1 mm was measured with a ruler. An anti-friction material was applied between the metal plate and the adhesive in order to produce a pre-cracked region.

2.2. Conditioning

Specimens were placed for ageing in a salt spray chamber. A solution of 5% mass sodium chloride [NaCl] was atomized at 200 ml/h and 35 °C. The exposure zone remained in a relative humidity between 95% and 98% and pH between 6.5 and 7.2, according to the ASTM B117 standard practice [30]. Specimen's top and bottom surfaces were covered with a layer of tape to avoid degradation of the adherends as shown in Fig. 2.

The average weight of 144.4 ± 1.7 g was measured from the specimens before ageing using a precision balance with 0.01 g. The ageing period was chosen based on the results of previous work with similar materials [13,14]. After an ageing period of 137 days, specimens were gently washed in clean running water and dried with paper and their weight was measured again.

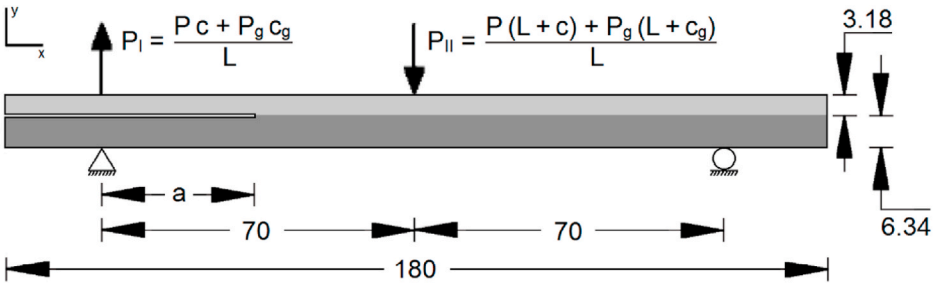

Fig. 4. Model geometry and contour conditions.

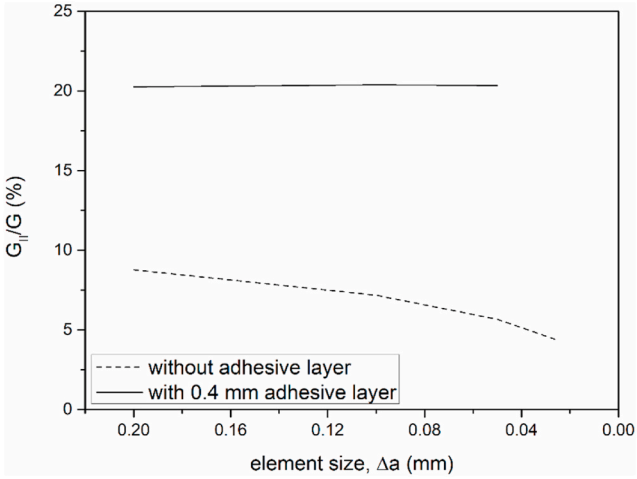

Fig. 5. Mesh sensitivity analysis.

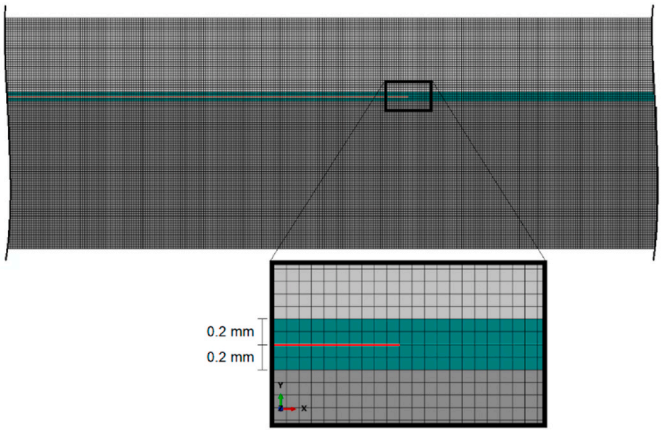

Fig. 6. Detail of the FE mesh around crack tip.

2.3. Experimental method

The MMB test was chosen for the experimental mixed-mode fracture analysis of the specimens. During the procedure, loading is applied from a yoke to rollers attached to a lever and loaded just above the mid-plane of the test specimen, as shown in Fig. 3. The test loading (P) is decomposed in opening (P_I) and shear (P_{II}) loadings in a constant ratio determined by the lever length (c). The mode I fracture ratio increases with the lever length. The lever weight produces a load (P_g) on the specimen at the length of the lever center of gravity (c_g). The test half-span (L) is set to 70 mm and the initial crack length (a) is 30 mm. The MMB test configuration produces higher stresses in the upper side of the specimen. Therefore, specimens were tested with the metal arm on top in order to prevent crack propagation within the composite material.

End-blocks of the same width as the specimens were bonded on both sides of the specimens using a structural epoxy adhesive. A thin layer of white correction fluid was coated on the specimen sides and millimeter paper was bonded in order to facilitate crack length measurements. Tests were conducted using a servo-hydraulic testing machine (MTS 831, MTS Systems Corporation, United States of America) equipped with a 10 kN load cell. The testing load was applied at a quasi-static rate with a controlled displacement of 0.5 mm/min. Load-displacement points were obtained during the tests and a high-resolution camera, synchronized with the test output data, is positioned for crack length monitoring.

3. Fracture data analysis

3.1. Numerical model

A 2D finite element (FE) model was developed in Abaqus Standard. The geometry was modelled based on the specimen measurements, as presented in Fig. 4. Loadings and contour conditions were applied in order to simulate the MMB test conditions. Boundary condition were defined by constraining displacements in x and y directions at the left side and displacements in y direction at the right side of the beam. The opening and shear loadings were applied at the top surface. Isotropic materials were selected from the properties presented in Table 1. A FE mesh of 4-node bilinear plane strain quadrilateral solid elements (CPE4) was applied in the whole model for optimized computational costs.

The calculation of the fracture energy was performed using the finite element method with the virtual crack closure technique (FEM/VCCT). The VCCT is based on linear elastic fracture mechanics (LEFM). This is valid as long as the energy dissipated on the fracture process zone (FPZ) ahead of the crack tip is in a small scale in relation to the macroscopic elastic response. In this work, the tested specimens have relatively thick adherends which increase the elastic response on a macroscopic scale. Additionally, the use of a thin adhesive layer with a brittle epoxy adhesive contributes for a smaller plastic zone.

A mesh sensitivity analysis was performed using the model of the MMB test with a crack length (a) of 30 mm. Elements of the same size were used on both sides of the crack and the aspect ratio of the elements in the vicinity of the crack tip was maintained at 1/1. The numerical analysis takes into consideration the effects of geometric nonlinearity. Results are shown in Fig. 5. The calculated fracture mode ratio (G_{II}/G) of a model without the adhesive layer showed dependency on the element size around the crack tip (Δa) and did not represent the actual fracture

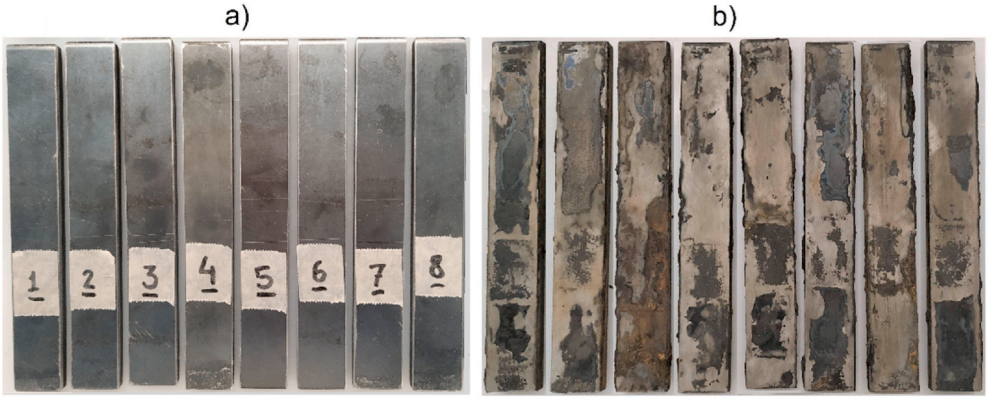

Fig. 7. Steel outer surface (a) non-aged and (b) aged conditions.

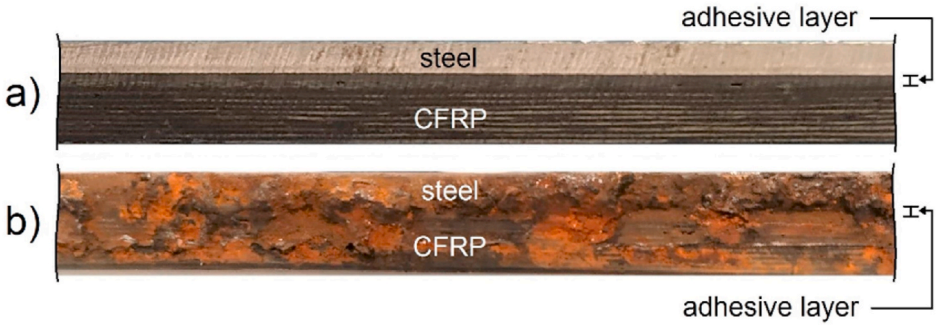

Fig. 8. Side view of a section of (a) non-aged and (b) aged specimens.

Table 2
Test matrix.

Specimen	Condition	Lever length, c (mm)	Lever weight, P_g (N)	Lever center of gravity, c_g (mm)
01–04	non-aged	110	17.6	40
05–08	non-aged	150	28.7	130
09–12	aged	110	17.6	40
13–16	aged	150	28.7	130

development. In order to circumvent the problem, literature suggests modelling an artificial interlayer around the crack [28,29]. Therefore, thin layers of 0.2 mm thickness with adhesive properties (see Table 1) were modelled on both sides of the crack. The effect of the adhesive layer on the stiffness of the arms is negligible. The calculated fracture mode (G_{II}/G) of the model with adhesive layer is independent from the element size. A global mesh with elements of 0.1 mm was chosen for the determination of the fracture energy at the load-crack length points, as shown in Fig. 6.

3.2. Analytical model

The strain-based partitioning method (SBM) [29] is based on beam analysis and allows determining the fracture mode and total fracture energy of bi-material cracks. The method requires a design condition of longitudinal strain equivalence between the sides of the crack to be satisfied. This means, under bending loadings:

$$E_U h_U^2 = E_L h_L^2 \quad (1)$$

Where E_U h_U, E_L and h_L are the flexural modulus and the thickness of the upper and lower arms, respectively. The SBM assumes that pure mode II is produced when the longitudinal strain distribution at the faying

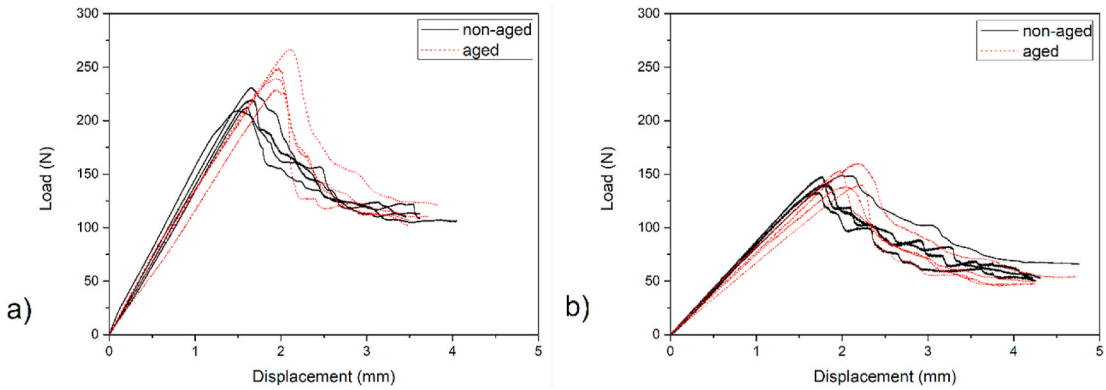

Fig. 9. Load-displacement curves of tests with lever length of (a) 110 mm and (b) 150 mm.

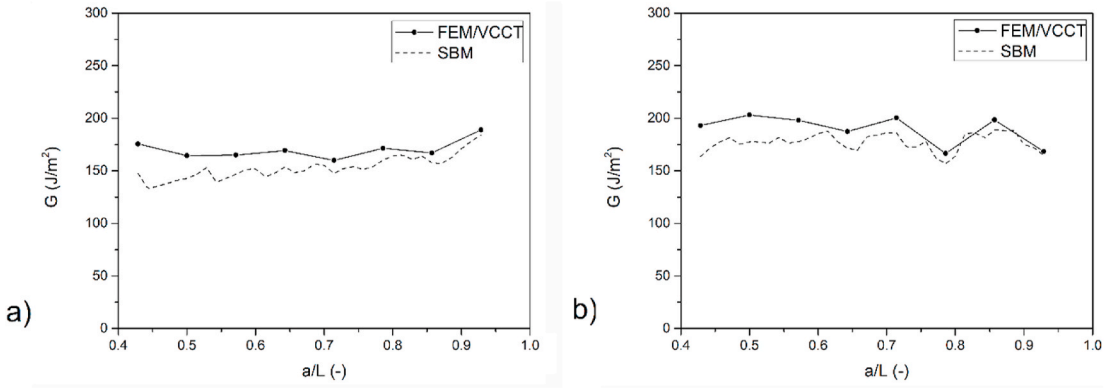

Fig. 10. Fracture energy of a representative specimen tested at a lever length of (a) 110 mm and (b) 150 mm.

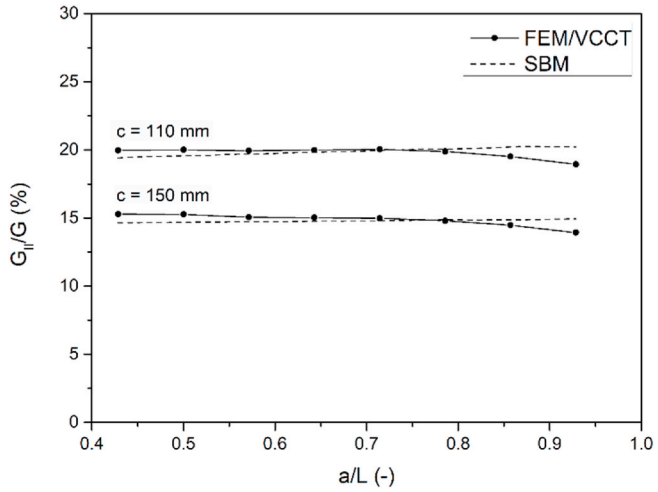

Fig. 11. Fracture mode ratio.

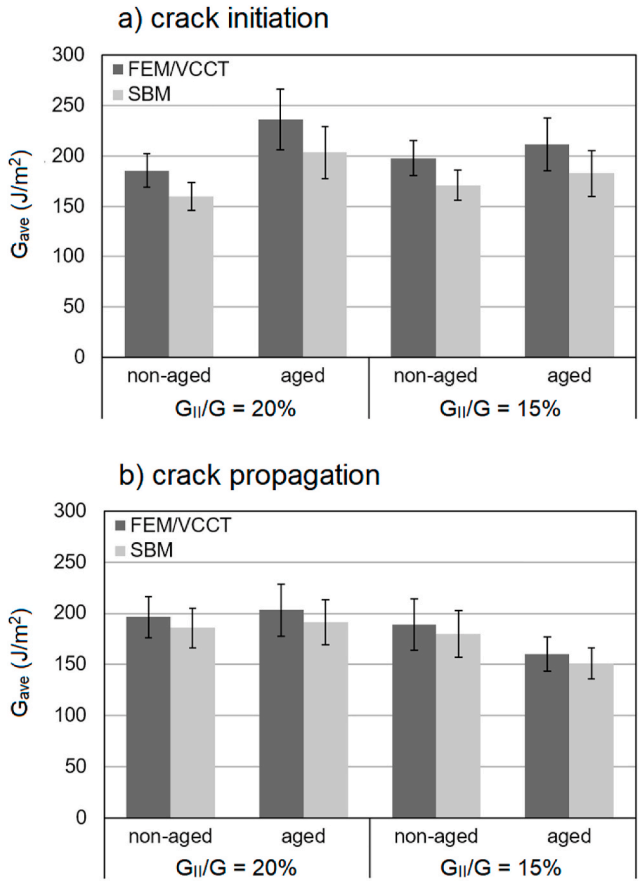

Fig. 12. Average fracture energy at (a) crack initiation and (b) propagation.

surfaces of both arms must be identical, and pure mode II is obtained when the curvatures in the two arms are the same [29]. The mode I, mode II and total fracture energy of MMB test specimens can be obtained by the following equations:

$$G_I = \frac{(\psi M_U - M_L)^2}{2B(\psi+1)^2}\left(\frac{1}{E_U I_U} + \frac{1}{E_L I_L}\right) \quad (2)$$

$$G_{II} = \frac{(M_U + M_L)^2}{2B(\psi+1)}\left(\frac{1}{E_U I_U} + \frac{(\psi+1)}{EI}\right) \quad (3)$$

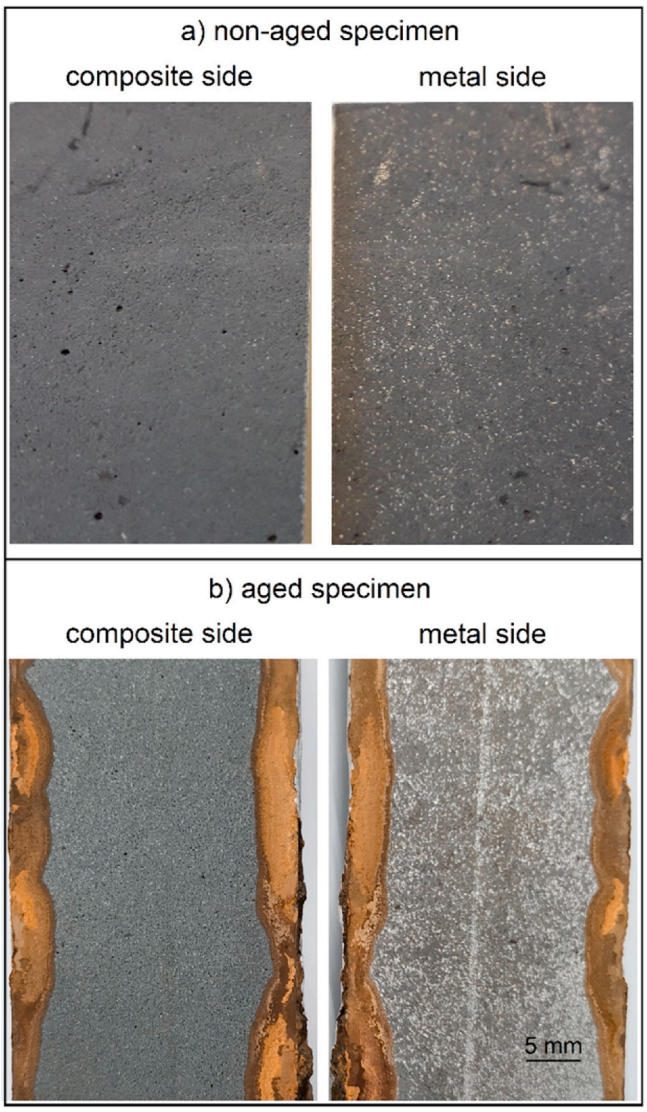

Fig. 13. Fracture surfaces of (a) non-aged and (b) aged specimens.

$$G = G_I + G_{II} \quad (4)$$

Where B is the specimen's width, M_U and M_L are the bending moments at the section of the crack tip in the upper and lower arms, respectively. E is the flexural modulus of the beam, I_U, I_L and I are the second moments of the area at the section of the crack tip in the upper arm, lower arm and beam, respectively. The bending stiffness ratio between the upper and lower arms is given by:

$$\psi = \frac{E_L I_L}{E_U I_U} \quad (5)$$

The SBM is a promising method for the easy and reliable fracture characterization of bi-material bonded joints [31].It is important to notice that the method requires linear-elastic conditions. The same parameters used in the FE model were applied to the calculation of the fracture energy using the SBM. Material properties were selected from Table 1 and geometrical parameters are indicated in Fig. 4. Moreover, Eqs. (2) and (3) do not consider effects of shear and crack tip rotations that are accounted in the numerical method.

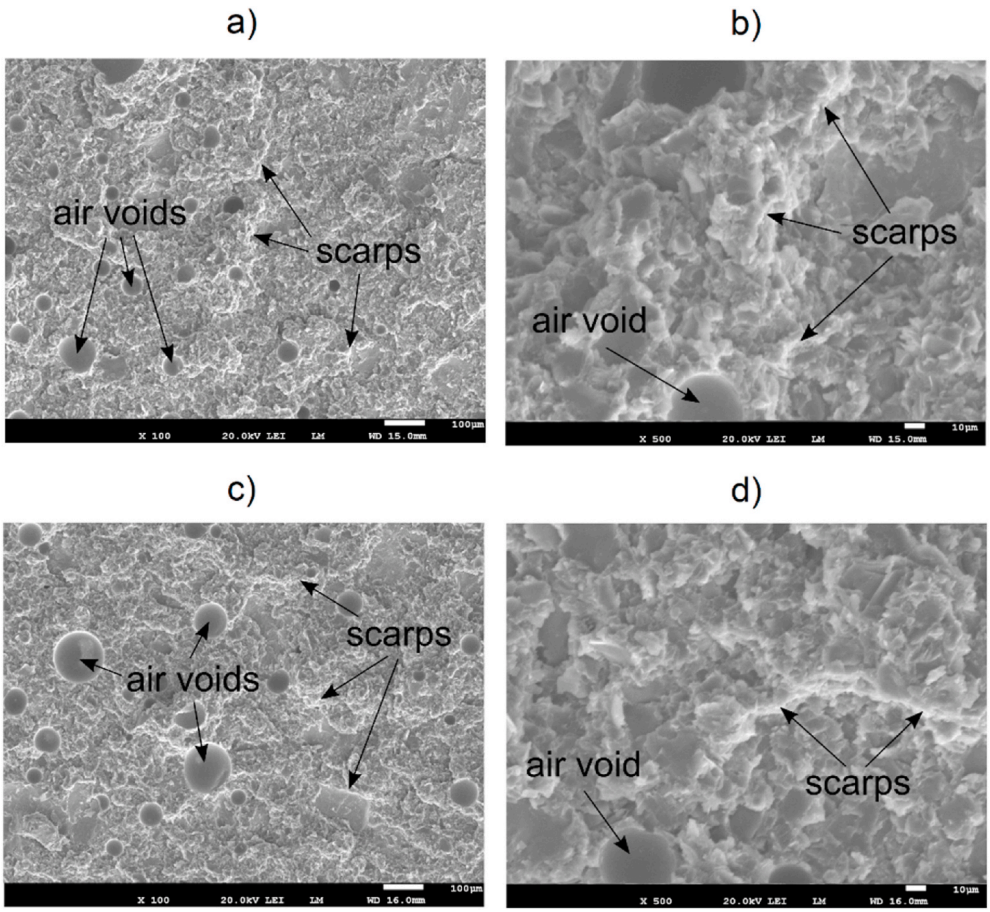

Fig. 14. SEM images of non-aged specimen tested with c = 110 mm (20% mode II) at (a) x100 and (b) x500 and tested with c = 150 (15% mode II) mm at (c) x100 and (d) x500.

4. Results and discussion

4.1. Effect of ageing on the materials

Fig. 7 shows the outer surface of the steel arm of non-aged and aged specimens. The effect of corrosion on the outer steel surface is negligible. This can be observed by comparing non-aged specimens (Fig. 7a) with the condition after ageing (Fig. 7b). The application of tape on the outer surfaces of the specimens showed to be effective in diminishing the degradation of metal adherends aged in salt fog. However, the average weight measured from the aged specimens is 142.9 ± 1.7 g, which means a decrease of 1.1% of the initial weight. This shows that the weight reduction due to corrosion of the steel member under long-term exposure to harsh environmental conditions had dominant effect against the weight increase due to moisture absorption of the adhesive [4] and the composite laminate [11]. These combined parameters make it difficult to determine the degree of moisture saturation at the bonded interface based on the measured weight during the conditioning process.

The effect of corrosion is noted on the sides of specimens, as shown in Fig. 8. The presence of corrosion products is observed over the metal and composite sides of aged specimens (Fig. 8b), in comparison with the non-aged sample (Fig. 8a). This shows the degradation of the sides of the steel member exposed during the ageing period. Literature states the galvanic corrosion of the composite material occurs as consequence of corrosion product depositions, acting as electric bridges between steel and exposed carbon fibers [17]. Overall, only the sides of the specimens were significantly affected by the ageing conditions.

4.2. Test results

Non-aged and aged specimens were tested using the MMB test method described in section 2.3. Aged specimens were abraded on the sides with sandpaper prior to the experiments to ensure accurate crack length monitoring during tests. Tests were performed in two different configurations, i.e., two lever lengths, as shown in Table 2. The lever length of 110 mm is the limitation obtained from the numerical model for which linear elastic behavior of the metal arm is guaranteed and the SBM can be evaluated for the fracture characterization. The lever length of 150 mm corresponds to the maximum length of the available equipment.

Fig. 9 shows the load-displacement curves obtained from the MMB tests. Composite-to-metal bonded joints exhibited typical curves, similar to standard symmetric specimens subjected to ageing conditions [25]. Results of non-aged and aged specimens tested with a lever length of 110 mm are presented in Fig. 9a. It can be noticed that the maximum load achieved by the aged sample is higher than the non-aged ones. This means that the bonded structure required higher loadings for crack initiation after ageing in saline atmosphere. However, specimens tested with a lever length of 150 mm presented similar curves in both non-aged and aged condition, as shown in Fig. 9b. The ageing process did not affect the performance of the bonded joint when tested at 150 mm. The overall stiffness of the structure was hardly affected by the ageing conditions, given the reduced effect of corrosion at the steel member (see Fig. 7) as well as the stability of carbon fibers in the presence of moisture [12]. Moreover, the effect of galvanic coupling seems to be negligible to the stiffness of the laminate.

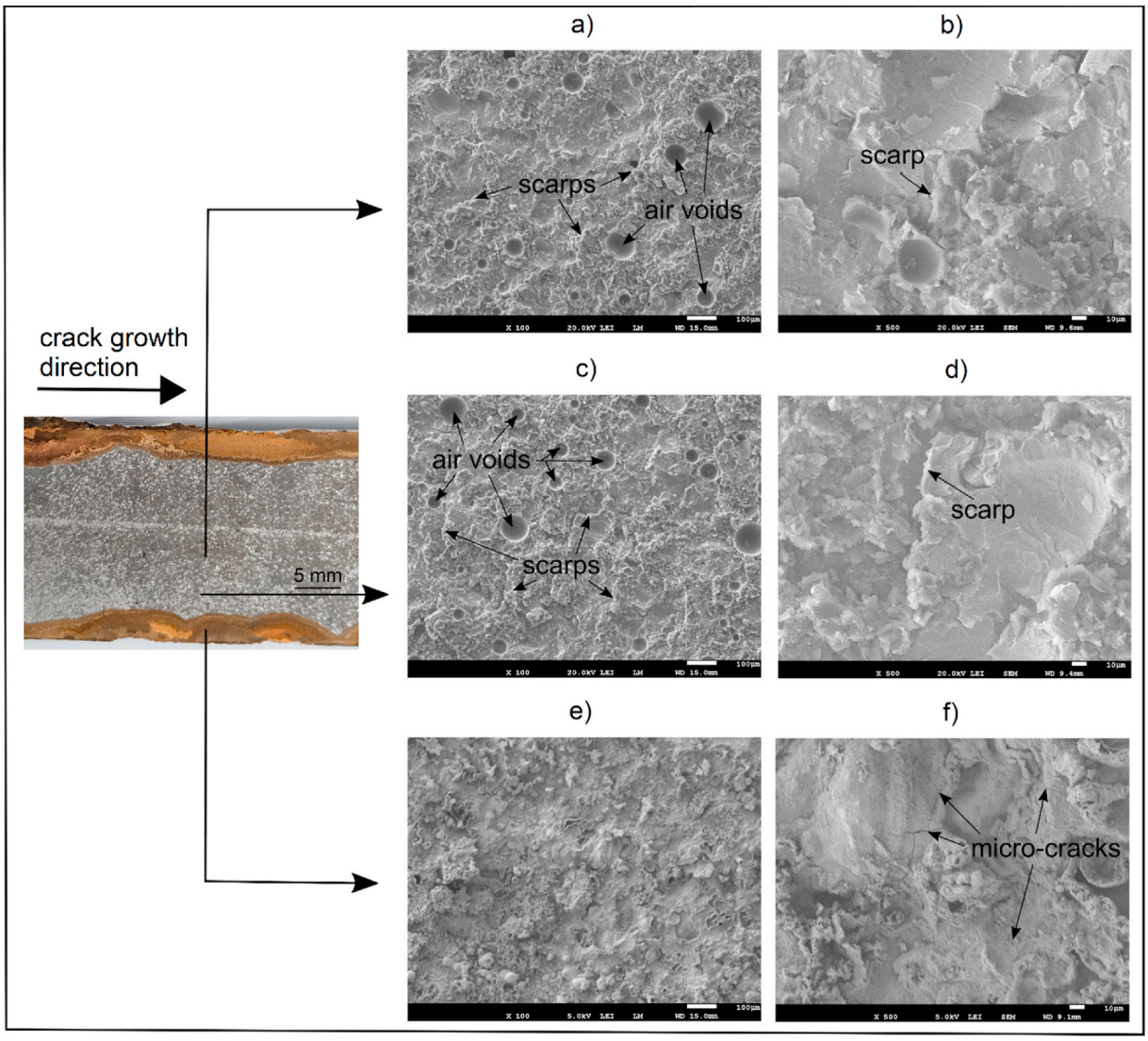

Fig. 15. SEM images of aged specimen in 100x and 500x, respectively, at (a, b) center, (c, d) intermediate and (e, f) edge regions of the fracture surface.

4.3. *Fracture toughness*

The effect of ageing on the interface fracture of the bonded materials is measured by the variation of the fracture toughness. It is assumed that the mechanical properties of the adherends remain the same after the ageing process. Therefore, only the adhesion mechanisms are considered in the analysis. The fracture toughness was obtained in terms of the total fracture energy (G) and the fracture mode ratio (G_{II}/G) using the numerical and analytical methods described in sections 3.1 and 3.2, respectively. The numerical results were calculated every 5 mm and the analytical results were calculated every 1 mm of the crack propagation.

Fig. 10 shows comparative results of the fracture energy obtained from the FEM/VCCT and the SBM in the two different testing configurations. Numerical values of the total fracture energy are shown to be consistent along crack propagation. Results calculated using the SBM deviated by 15% from the FEM/VCCT at crack initiation and converged as the crack length increases. This is attributed to the effect of shear stresses that are not considered in the SBM but can be significant when testing beams with high thickness-to-span ratio [29].

The fracture mode ratio obtained from numerical and analytical methods is presented in Fig. 11. Numerical results (FEM/VCCT) presented nearly constant results along the crack propagation with a slight reduction of the mode II portion at the crack propagation points near the specimen half-length. In addition, the global mode ratio at the whole specimen, obtained from the SBM, showed good agreement with the local mode ratio at the crack tip, obtained from the numerical simulations. This indicates that the effect of the FPZ is negligible. The SBM predicted, with accuracy, the partitioning ratio of the composite-to-metal bonded joints. The test configuration with a lever length of 110 mm produced 20% mode II and the lever length of 150 mm resulted in 15% mode II fracture ratio.

The average fracture energy (G_{ave}), presented in Fig. 12, provides a comparable data for the evaluation of the ageing effect on the fracture performance of the tested specimens. Fig. 12a shows the mean fracture energy at crack initiation of the 4 repeats of each configuration. It reveals a significant increase of 27% of the fracture energy at crack initiation when tested in 20% mode II. In the case of specimens tested in 15% mode II, the fracture energy showed a slight increase of 7% at crack initiation. The region of crack initiation is directly affected by the moisture across the whole width and resulted in an increase of the fracture toughness. This seems to be related to the shear behavior of the adhesive and is attributed to the effect of plasticization [19,21].

Fig. 12b shows the mean fracture energy at crack propagation points (from 35 to 65 mm crack length) of the 4 repeats of each configuration. A negligible variation is observed of 3% of the fracture energy at 20% mode II during crack propagation, while a reduction 15% of the fracture

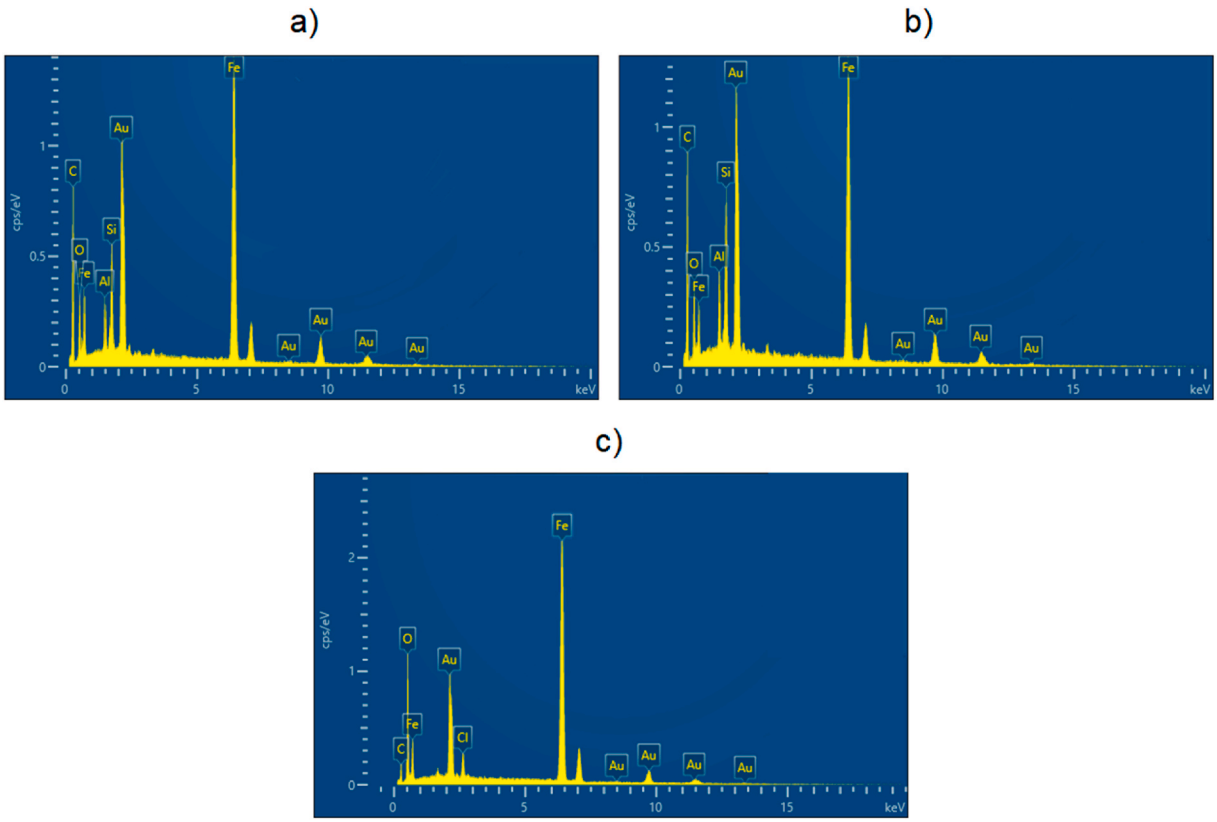

Fig. 16. EDS of aged specimen at (a) center, (b) intermediate and (c) edge regions.

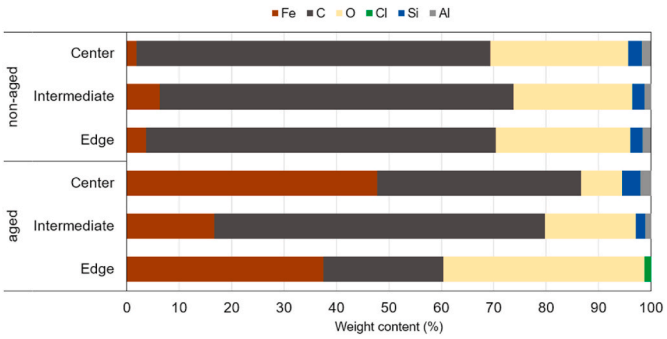

Fig. 17. EDS of aged specimen at center, intermediate and edge regions of the fracture surface.

energy is noted at 15% mode II. As expected, the SBM showed good agreement with the numerical results. Moreover, the average fracture energy obtained from the SBM deviated by 15% from the FEM/VCCT at crack initiation (Figs. 12a) and 6% during propagation (Fig. 12b), as observed in Fig. 10.

4.4. Fractography

Representative images of the fracture surfaces are presented in Fig. 13. Both non-aged and aged specimens presented most of the adhesive stuck to the composite adherend (lower surface), while a thin layer of adhesive remained on the metal side (upper surface). Overall, the non-aged specimens (Fig. 13a) exhibited thin-layer cohesive failure as the triggering failure mode. This observation confirms good bond quality and ensures high joint efficiency. In the case of the aged specimens (Fig. 13b), moisture penetration is noticed on both side edges of the fracture surfaces.

A detailed analysis of the fracture surfaces was performed using a field emission scanning electron microscope (SEM) (JSM-7500F, JEOL, Japan). Prior to examination, samples were coated with two ultra-thin (15 μm) layers of gold using a sputtering system (Q300T D, Quorum Technologies, United Kingdom) for the SEM analysis of non-conductive materials. Fig. 14 shows typical fracture surfaces from the metal side of non-aged specimens using magnifications of 100 and 500 times. Crack propagation direction is from the left to the right side of the images. Both test configurations of 20% mode II (Fig. 14a and b) and 15% mode II (Fig. 14c and d) demonstrated similar surfaces of cohesive failure with the presence of air voids and scarps. These features confirm that the fracture occurred with dominant mode I loadings in both test configurations [11,14]. No significant difference in the failure mechanisms was noticed between the two mode ratios.

Fig. 15 shows the fracture surfaces from the metal side of an aged specimen using magnifications of 100 and 500 times. Images were obtained in three different regions: at the center of the surface, near the edge, and in an intermediate region. Images from the center (Fig. 15a and b) and intermediate (Fig. 15c and d) regions show the presence of adhesive attached to the metal surface indicating cohesive failure, such as the non-aged specimens in Fig. 14. However, slight less scarps on the adhesive surface can be observed, indicating a certain variation of the failure mechanism in these regions. Images obtained from regions affected by moisture (Fig. 15e and f) showed remarkably distinct fracture surfaces of seemingly adhesive failure. The occurrence of microcracks observed at high magnification (Fig. 15f) indicates the presence of corrosion products at the interface due to the degradation of the metal adherend.

In order to have a better understanding of the failure mechanisms, a chemical characterization was performed by using Energy-Dispersive Spectroscopy (EDS), available in the SEM equipment. Fig. 16 shows the chemical spectrum of the regions presented in Fig. 15, in terms of counts per second per electron-volt (cps/eV). Results reveal the presence

of chloride [Cl] in the region of moisture penetration near the edge of the fracture surfaces (Fig. 16c), while it was not found at the center and intermediate regions (Fig. 16a and b). The incidence of salt traces at the fracture surface is an indication of adhesive failure due to degradation and ingress of salt within the interface [28]. Additionally, the higher content of iron [Fe] and oxygen [O] elements confirm the presence of corrosion products at the interface, as noticed in Fig. 15e and f. Moreover, minor amounts of aluminum [Al] and silicon [Si] contaminations are observed at the center and intermediate regions. The presence of these elements can be attributed to the surface preparation of the metal adherend.

Fig. 17 shows the relative weight content of the chemical components at the fracture surfaces of non-aged and aged specimens. The gold [Au] content was excluded from this analysis. The non-aged specimens demonstrated a high content of carbon [C] and oxygen [O] elements in contrast to the slight presence of iron [Fe], which shows the dominant presence of adhesive in the fracture surfaces. In the case of aged specimens, the increased incidence of iron [Fe] indicates an exposed metal interface at center and intermediate regions. This suggests a combination of cohesive and adhesive failure in regions unaffected by the moisture, occurred closer to the interface with the incidence of the interfacial fracture.

The results obtained from the fractographic analysis help to explain the effect of salt spray ageing on the mechanical behavior of the bonded joint. The failure mode shifted from thin-layer cohesive to adhesive failure in the regions where the ingress of moisture and salt is observed. Additionally, the ageing process also affected the metal-adhesive interface in regions where the ingress of moisture was not observed, changing from thin-layer cohesive failure to a combination of thin-layer cohesive and adhesive failure. This degradation mechanism is important since a very long exposure time is needed in order to have a significant penetration of moisture within the interface. Therefore, the decrease of the fracture toughness observed at crack propagation can be related to the degradation of the interfacial adhesion between metal adherend and adhesive. Moreover, the increase of the fracture toughness observed at crack initiation may be related mainly to the mechanical behavior of the adhesive material than the failure mode.

5. Conclusion

The effect of long-term environmental exposure on the performance of composite-to-metal bonded joints was investigated. Bi-material bonded specimens with steel and CFRP adherends were manufactured and aged in salt fog. MMB tests were performed for non-aged and aged specimens and the mixed-mode fracture ratios were obtained using the virtual crack closure technique (FEM/VCCT) and the strain-based method (SBM). The fracture surfaces were analyzed in order to evaluate the failure mechanisms and their association with the performance of the bonded materials subjected to environmental exposure.

The metal adherend suffered significant damage during ageing in salt spray environment. The combined effects of corrosion on the metal and moisture uptake on the adhesive and composite made it difficult to determine the degree of moisture saturation at the bonded interface based on the measured weight during the conditioning process. Overall, the long-term exposure to salt spray environment did not have a drastic effect on the adhesive layer although it was extremely aggressive to the steel adherend. The presence of corrosion products resulted from the steel degradation was observed at the sides of the specimens and at the interface, together with the salt and moisture.

The strain-based method (SBM) predicted, with accuracy, the fracture mode ratio of bi-material bonded joints. It proved to be an easy and reliable solution based on closed form equations with parameters obtained directly from the experiments that allows the characterization of fracture behavior of cracks between different materials. In contrast, the use of numerical solutions requires the use of complex models and high computational costs.

Non-aged specimens demonstrated thin-layer cohesive failure occurring near the metal adherend. The effect of ageing resulted in an increase of the fracture toughness at crack initiation. This seems to be related to the shear behavior and plasticization of the adhesive. At the same time, the penetration of moisture at the edges of the fracture surface produced adhesive failure in these regions affected by moisture. Additionally, the failure mode at the unaffected regions of the fracture surface of aged specimens shifted from thin-layer cohesive failure to a combination of thin-layer cohesive and adhesive failure. This may explain the typical changes of the mechanical behavior of bonded joints at initial stages of ageing followed by a steady condition when pure adhesive failure is reached.

Acknowledgements

This work was supported by the Coordenação de Aperfeiçoamento de Pessoal de Nível Superior - Brasil (CAPES), Conselho Nacional de Desenvolvimento Científico e Tecnológico (CNPq), Fundação Carlos Chagas Filho de Amparo à Pesquisa do Estado do Rio de Janeiro (FAPERJ) [001], and is based upon work from COST Action CA18120 (CERTBOND - https://certbond.eu/), supported by COST (European Cooperation in Science and Technology - https://www.cost.eu/).

References

[1] Budhe S, Banea MD, de Barros S. An updated review of adhesively bonded joints in composite materials. Int J Adhesion Adhes 2017;72:30–42. https://doi.org/10.1016/j.ijadhadh.2016.10.010.
[2] Oudad W, Madani K, Bouiadjra B Bachir, Belhouari M, Cohendoz S, Touzain S, Feaugas X. Effect of humidity absorption by the adhesive on the performances of bonded composite repairs in aircraft structures. Compos. Part B 2012;43:3419–24. https://doi.org/10.1016/j.compositesb.2012.01.028.
[3] Lau D, Büyüköztürk O. Fracture characterization of concrete-epoxy interface affected by moisture. Mech Mater 2010;42:1031–42. https://doi.org/10.1016/j.mechmat.2010.09.001.
[4] Viana G, Costa M, Banea MD, da Silva LFM. A review on the temperature and moisture degradation of adhesive joints. Proc Inst Mech Eng, Part L 2017;231(5):488–501. https://doi.org/10.1177/1464420716671503.
[5] Brewis DM, Comyn J, Shalash RJA. The effect of moisture and temperature on the properties of an epoxide-polyamide adhesive in relation to its performance in single lap joints. Int J Adhesion Adhes 1982;2(4):215–22. https://doi.org/10.1016/0143-7496(82)90028-8.
[6] Pethrick RA. Design and ageing of adhesives for structural adhesive bonding – a review. Proc Inst Mech Eng, Part L 2015;229(5):349–79. https://doi.org/10.1177/1464420714522981.
[7] Sugiman S, Crocombe AD, Aschroft IA. Experimental and numerical investigation of the static response of environmentally aged adhesively bonded joints. Int J Adhesion Adhes 2013;40:224–37. https://doi.org/10.1016/j.ijadhadh.2012.08.007.
[8] Papanicolaou GC, Charitidis P, DE Mouzakis, Karachalios E, Jiga G, Portan DV. Experimental and numerical investigation of balanced Boron/Epoxy single lap joints subjected to salt spray aging. Int J Adhesion Adhes 2016;68:9–18. https://doi.org/10.1016/j.ijadhadh.2016.01.009.
[9] Park Y-B, Song M-G, Kim J-J, Kweon J-H, Choi J-H. Strength of carbon/epoxy composite single-lap bonded joints in various environmental conditions. Compos Struct 2010;92:2173–80. https://doi.org/10.1016/j.compstruct.2009.09.009.
[10] Jeong M-G, Kweon J-H, Choi J-H. Effect of various hygrothermal environments on the failure of adhesively bonded composite single-lap joints. J Compos Mater 2013;47:2061–73. https://doi.org/10.1177/0021998312453357. 17.
[11] Arouche MM, Budhe S, Banea MD, Teixeira de Freitas S, de Barros S. Interlaminar adhesion assessment of carbon-epoxy laminates under salt water ageing using peel tests. Proc Inst Mech Eng, Part L 2019. https://doi.org/10.1177/1464420718766626.
[12] Mariam M, Afendi M, Abdul Majid MS, Ridzuan MJM, Azmi AI, Sultan MTH. Influence of hydrothermal ageing on the mechanical properties of an adhesively bonded joint with different adherends. Compos. Part B 2019;165:572–85. https://doi.org/10.1016/j.compositesb.2019.02.032.
[13] Arouche MM, Budhe S, Alves LA, Teixeira de Freitas S, Banea MD, de Barros S. Effect of moisture on the adhesion of CFRP-to-steel bonded joints using peel tests. J Braz Soc Mech Sci Eng 2018;40:10. https://doi.org/10.1007/s40430-017-0959-6.
[14] Teixeira de Freitas S, Banea MD, Budhe S, de Barros S. Interface adhesion assessment of composite-to-metal bonded joints under salt spray conditions using peel tests. Compos Struct 2017;164:68–75. https://doi.org/10.1016/j.compstruct.2016.12.058.
[15] Heshmati M, Haghani R, Al-Emrani M. Durability of bonded FRP-to-steel joints: effects of moisture, de-icing salt solution, temperature and FRP type. Compos. Part B 2017;119:153–67. https://doi.org/10.1016/j.compositesb.2017.03.049.

[16] Sugiman S, Setyawan PD, Salman S, Ahmad H. Experimental and numerical investigation of the residual strength of steel-composites bonded joints: effect of media and aging condition. Compos. Part B 2019;173:106977. https://doi.org/10.1016/j.compositesb.2019.106977.
[17] Yang Y, Silva MAG, Silva RJC. Material degradation of cfrp-to-steel joints subjected to salt fog. Compos. Part B 2019;173:106884. https://doi.org/10.1016/j.compositesb.2019.05.095.
[18] Loh WK, Crocombe AD, Abdel Wahab MM, Ashcroft IA. Environmental degradation of the interfacial fracture energy in an adhesively bonded joint. Eng Fract Mech 2002;69:2113–28. https://doi.org/10.1016/S0013-7944(02)00004-8.
[19] Wylde JW, Spelt JK. Measurement of adhesive joint fracture properties as a function of environmental degradation. Int J Adhesion Adhes 1998;18(4):237–46. https://doi.org/10.1016/S0143-7496(98)00028-1.
[20] Ameli A, Papini M, Spelt JK. Fracture R-curve of a toughened epoxy adhesive as a function of irreversible degradation. Mater. Sci. Eng. A. 2010;527(20):5105–14. https://doi.org/10.1016/j.msea.2010.04.099.
[21] Fernandes P, Viana G, Carbas RJC, Costa M, da Silva LFM, Banea MD. The influence of water on the fracture envelope of an adhesive joint. Theor Appl Fract Mech 2017;89:1–15. https://doi.org/10.1016/j.tafmec.2017.01.001.
[22] Costa M, Viana G, da Silva LFM, Campilho RDSG. Effect of humidity on the mechanical properties of adhesively bonded aluminium joints. Proc Inst Mech Eng, Part L 2018;232(9):733–42. https://doi.org/10.1177/1464420716645263.
[23] Markatos DN, Tserpes KI, Rau E, Markus S, Ehrhart B, Pantelakis Sp. The effects of manufacturing-induced and in-service related bonding quality reduction on the mode-I fracture toughness of composite bonded joints for aeronautical use. Compos. Par B 2013;45:556–64. https://doi.org/10.1016/j.compositesb.2012.05.052.
[24] Fernandes RL, MFSF de Moura, Moreira RDF. Effect of moisture on pure mode I and II fracture behaviour of composite bonded joints. Int J Adhesion Adhes 2016;68:30–8. https://doi.org/10.1016/j.ijadhadh.2016.01.010.
[25] LeBlanc LR, LaPlante G. Experimental investigation and finite element modeling of mixed-mode delamination in a moisture-exposed carbon/epoxy composite. Compos. Part A 2016;81:202–13. https://doi.org/10.1016/j.compositesa.2015.11.017.
[26] Silva FGA, MFSF de Moura, Moreira RDF. Influence of adverse temperature and moisture conditions on the fracture behaviour of single-strap repairs of carbon-epoxy laminates. Int J Adhesion Adhes 2020;96:102452. https://doi.org/10.1016/j.ijadhadh.2019.102452.
[27] André A, Haghani R, Biel A. Application of fracture mechanics to predict the failure load of adhesive joints used to bond CFRP laminates to steel members. Construct Build Mater 2012;27:331–40. https://doi.org/10.1016/j.conbuildmat.2011.07.040.
[28] Shahverdi M, Vassilopoulos AP, Keller T. Mixed-mode I/II fracture behavior of asymmetric adhesively-bonded pultruded composite joints. Eng Fract Mech 2014;115:43–59. https://doi.org/10.1016/j.engfracmech.2013.11.014.
[29] Arouche MM, Wang W, Teixeira de Freitas S, de Barros S. Strain-based methodology for mixed-mode I+II fracture: a new partitioning method for bi-material adhesively bonded joints. J Adhes 2019;95:385–404. https://doi.org/10.1080/00218464.2019.1565756.
[30] ASTM B117-18. Standard practice of operation salt spray (fog) apparatus. ASTM International; 2018.
[31] Arouche MM, Teixeira de Freitas S, de Barros S. On the influence of glass fiber mat on the mixed-mode fracture of composite-to-metal bonded joints. Compos Struct 2021;256:113109. https://doi.org/10.1016/j.compstruct.2020.113109.